Volume 1 | Number 1 | Jan 2013 | Pages 1–100

Polymer Chemistry

www.rsc.org/polymers

ROYAL SOCIETY OF CHEMISTRY

ROYAL SOCIETY OF CHEMISTRY

www.rsc.org/polymers

Polymer Chemistry

ARTICLE

Novel Lanthanide-Polymer Complexes for Dye-Free Dual Modal Probes for MRI and Fluorescent Imaging

Fangyi Cao[a], Tongcun Huang[b], Yifei Wang[a], Fei Liu[b], Lumin Chen[b], Jun Ling[a, †], Jihong Sun[b, †]

High-resolution imaging is powerful in theranostic and staging of tumors. Dual-modal imaging using lanthanide hybrid nanoparticles as probes have been attracting increasing attention based on their specific and intrinsic physical properties. The present work reports a novel water-soluble micelle of an amphiphilic block copolymer with diketone pendants chelating gadolinium (Gd^{3+}) and europium (Eu^{3+}) cations as a dual probe of magnetic resonance imaging (MRI) and fluorescent imaging for clinical detection. The Gd^{3+} and Eu^{3+} hybrid micelles have a homogeneous size distribution and hydrodynamic diameters tunable between 80 and 220 nm. Macromolecular diketone ligand enhances relaxation rate of Gd^{3+} and sensitizes Eu^{3+} luminescence efficiently. Further sensitized by the co-doped Gd^{3+}, Eu^{3+} complex exhibits a long-lived emission with large Stokes shift. A strong red light at wavelength of 615 nm is observed with an excitation in the range of 350 and 405 nm. Cellular uptake experiments reveal excellent biocompatibility and rapid uptake of the nanoparticles by MCF-7 cells. The robust dual-modal probes are promising in applications on early diagnosis of tumor, presurgical planning, and intraoperative fluorescence-guided surgery.

Introduction

In the past years, dual modality imaging probes within a single molecule are attracting increasing attention in the field of molecular imaging since they offer synergistic advantages over any single outputs.[1, 2] Among the commonly used molecular bioimaging modalities, some are characterized by superb spatial resolution but low sensitivity and requiring high concentration of the contrast agents to be detected, for instance, magnetic resonance imaging (MRI). Others endow with high sensitivity and high contrast images but low resolution such as fluorescence imaging. MRI/Fluorescence bimodal imaging offers the merits of coupling the high sensitivity of fluorescence with the high resolution of MRI.[3-9]

Lanthanide chelates are well known as molecular imaging agents because of their unique magnetic and photophysical properties that can yield multi-modal signatures including line-like emission, long-living fluorescence and magnetic resonance. In lanthanide ions, Gd^{3+} is an attractive candidate for MRI contrast agents and probes due to the fact of its paramagnetism. The long electronic relaxation time of 10^{-8} to

10^{-9} s coupled with a high magnetic moment (7.9 μ_B) makes Gd^{3+} available for increasing and controlling the magnetic relaxation of water protons.[10] Eu^{3+} ions have remarkable luminescence characteristics, such as non-overlapped, easily recognizable and line-like emission bands in the visible region (500 to 700 nm), large stokes shift, as well as inherent long-lived excited states (ms domains) that prevent the interference from any spontaneous background emission sources.[11] It becomes promising fluorescence bioprobe over conventional organic dyes.[12] Many europium complexes with various β-diketones as sensitizer[13, 14] have received great interest due to the high absorbance coefficient of the ligand and efficient intramolecular energy transfer to Eu^{3+} cations. More interestingly, a co-doped Gd/Eu in a matrix can readily sensitize the emission of Eu^{3+} efficiently.[15, 16] In Gd/Eu hybrid probes for MRI and fluorescent imaging, various ligands have been developed for their magnetic or optical properties.[17]

Recently, many research groups developed different molecules to chelate Ln^{3+} for MRI/fluorescent imaging including aminopolycarboxylic open-chain ligands and macrocyclic derivatives of 1,4,7,10-tetraazacyclododecane-1,4,7,10-tetraacetic acid (DOTA).[18, 19] For example, Petoud and Tóth reported two prototype pyridine-based lanthanide complexes that addressed requirements for both MRI and luminescence imaging and demonstrated that the presence of two H_2O molecules bound to the Gd^{3+} beneficial for MRI applications analogue.[3, 20] Similarly, Laurent et al. prepared Gd and Eu complexes of PMN-tetraacetic acid showing interesting properties both for a high proton relaxivity with favorable water residence time and long luminescence lifetime.[21]

a. MOE Key Laboratory of Macromolecular Synthesis and Functionalization, Department of Polymer Science and Engineering, Zhejiang University, Hangzhou 310027, China.
b. Department of Radiology, Sir Run Run Shaw Hospital, School of Medicine, Zhejiang University, Hangzhou 310016, China.
† Correspondence author, email: lingjun@zju.edu.cn (J.L.), braversun@sina.com (J.S.)
Electronic Supplementary Information (ESI) available: [details of any supplementary information available should be included here]. See DOI: 10.1039/x0xx00000x

ARTICLE

Meanwhile, as the gadolinium based MRI technique suffers from low sensitivity in small molecules. One common method to lower the tumbling rate of Gd^{3+} is conjugating Gd^{3+} to macromolecules like linear polymers or dendrimers.[22-26] Another approach to improve the sensitivity is the accumulation of Gd^{3+} agents in a small volume by introducing Gd^{3+} into supramolecular aggregates like micelles or liposomes.[27] Making a bimodal probe of MRI/fluorescent imaging in macromolecules is a new strategy to reduce the tumbling rate of Gd^{3+} and to encapsulate many Gd^{3+} ions in a nano-scaled volume at the same time.

Parac-Vogt succeeded in using novel diethylenetriaminepentaacetic acid (DTPA) based amphiphilic derivatives as model contrast agents for bimodal imaging.[27] Among the reported organic ligands, β-diketone ligands are well known as a sensitizer utilized for lanthanide complexes. Furthermore, β-Diketone containing ligands are easy to synthesize and can chelate both Gd^{3+} and Eu^{3+}. By this approach, high resolution of magnetic resonance imaging of gadolinium and the high sensitivity of europium fluorescent imaging are combined in one single probe for combined diagnostic technique.

Herein, we report the synthesis of novel well-defined diblock copolymers poly[4-(3-oxo-3-phenylpropanoyl)phenyl methacrylate]-*b*-poly[oligo(ethylene glycol) methyl ether methacrylate] (PDKMA-*b*-POEGMA) with tunable chain lengths by reversible addition fragmentation chain transfer (RAFT) polymerization. Both the monomer and block copolymers can be easily prepared. The amphiphilic block copolymers self-assemble into micelles in aqueous solution and chelate lanthanide cations (both Gd^{3+} and Eu^{3+}) at the same time to realize bimodal imaging of MRI and fluorescence. Due to the hydrophobic core of micelle, the non-radiative deactivation of Eu^{3+} fluorescence is suppressed. The cochelated Gd^{3+} also sensitizes Eu^{3+} fluorescence. Meanwhile, high longitudinal relaxivity values are obtained attributed to outer sphere interactions of micelles.

Experimental

Materials

Methacryloylchloride (Mingxing Chemical Co.) was distilled under reduced pressure before use. 1-(4-Hydroxyphenyl)ethanone (Energy Chemical), methyl benzoate (Sinopharm Chemical Reagent), triethylamine (TEA) was distilled over CaH_2. Tetrahydrofuran (THF) was refluxed over potassium/benzophenone ketyl prior to use. 2,2'-Azoisobutyronitrile (AIBN, 98%, Aldrich) was recrystallized from ethanol. Cumyl dithiobenzoate (CDB) was synthesized as reported.[28] Oligo(ethylene glycol) methyl ether methacrylate (OEGMA, M_n = 500 g/mol, Aldrich) was deinhibited by passing through basic alumina columns before polymerizations. Rare earth metal oxides (Gd_2O_3, Eu_2O_3) were purchased from Beijing Founde Star Science and Technology Co. Ltd. and transformed to corresponding rare earth metal ions (Ln^{3+}) through reaction with acid at elevated temperature. All other solvents and chemicals were of analytic grade and used as received.

Cells

Human breast carcinoma MCF-7 cells were cultured in tissue culture flasks with medium RPMI 1640 supplemented with 10% fetal bovine serum (FBS) under a 5% CO_2 atmosphere at 37 °C. After reaching 80% confluence, the cells were collected from flasks with trypsin/EDTA treatment. Cell suspensions were seeded into 96-well cell culture plates at a cell density of 8000 cells/well. After incubation for 24h, the cells were used for the cytotoxicity tests.

Instruments and Measurements

Nuclear magnetic resonance spectroscopy (NMR) were recorded on a Bruker Avance III 400 spectrometer (^{1}H: 400 MHz and ^{13}C: 100 MHz) at room temperature using $CDCl_3$ as solvent and tetramethylsilane (TMS) as internal reference. Gas chromatography-time of flight mass spectrometry (GC-TOFMS) spectrum was measured by GCT Premier, WATERS. MWs and Đ were determined by size exclusion chromatography (SEC) on a Waters-150C apparatus equipped with Waters Styragel HR3 and HR4 columns and a Waters 2414 refractive index detector. THF was used as the eluent with a flow rate of 1.0 mL/min at 40 °C. Triple-detection Size Exclusion Chromatography (Triple-SEC) measurements were conducted on SEC system equipped a Waters 515 pump, an autosampler and two MZ gel columns (103 Å and 104 Å) with a flow rate of 0.5 mL/min in THF at 25 °C. The MALS detector was used to determine the molecular weight. ASTRA software (Version 5.1.3.0) was utilized for acquisition and analysis of data. Differential scanning calorimetry (DSC) analyses were performed on a TA Q20 instrument. PDKMAs and PDKMA-*b*-POEGMAs were heated from room temperature to 175 °C at a rate of 10 °C/min under a nitrogen purge, held for 3 min to erase the thermal history, cooled to −50 °C at a rate of 40 °C/min, and finally subjected to a second scan at a rate of 10 °C/min. The second heating scan from −50 to 175 °C was then recorded. Thermogravimetric analysis (TGA) was performed on a TA Q50 instrument. Samples were heated from 50 °C to 500 °C at a rate of 10 °C/min. Dynamic light scattering (DLS) study of aqueous micellar nanoparticle solutions was determined using a particle size analyzer (Zetasizer Nano Series, Malvern Instruments) at 25 °C. Zeta potential studies of aqueous polymer micellar nanoparticle solutions were determined using a Nano-ZS 90 Nanosizer (Malvern Instruments Ltd.). Each reported measurement was conducted for three runs. Transmission electron microscopy (TEM) images of Ln^{3+} hybrid micellar nanoparticles were obtained using a HITACHI HT7700 instrument. FT-IR spectra were recorded on Bruker VECTOR 22. The measurements were performed on tablets containing KBr and sample. The absorbance spectra of the block copolymers and nanoparticles were recorded in the range of 3500-400 cm^{-1}. Inductively coupled plasma optical emission spectrometry (ICP-OES) was applied to determine the Ln^{3+} contents of the nanoparticles.

The measurements were conducted on a Thermo i CAP6300. Standard solutions of free rare earth metal cations were prepared as the references for the measurements. UV-Vis spectra were conducted on a UV-2450 UV-Vis spectrophotometer (SHIMADZU). The absorbance and transmittance spectra of the Ln^{3+}-loaded nanoparticles were recorded in the range of 250-600 nm. Photoluminescence (PL) excitation and emission spectra of the aqueous solutions of the Eu^{3+}-containing hybrid micellar nanoparticles were recorded by using a FluoroMax-4 spectrofluorometer (HORIBA). The Ln^{3+} concentration of each sample was previously determined by ICP-OES, as described above. A UV lamp operating at 350 nm was applied to record the luminescence images of hybrid nanoparticles. Magnetic resonance imaging (MRI) study was performed using a 3.0-T MRI system (Signa HDxt, GE Medical Systems, Milwaukee, WI, USA). The absorbance of CCK-8 was measured by using a microplate reader (BioRad, model 680, USA). The cellular uptake behavior of Ln^{3+}-loaded nanoparticles in MCF-7 cells was visualized under confocal laser scanning microscopy (CLSM) (OLYMPUS, BX61W1-FV1000).

Methods

Synthesis of 4-(3-oxo-3-phenylpropanoyl)phenyl methacrylate (DKMA). 1-(4-Hydroxyphenyl)-3-phenylpropane-1,3-dione (Intermediate) was synthesized as reported.[29] Intermediate (10.0 g, 40.8 mmol) was dissolved in 100 mL dry THF followed by adding TEA (6.8 mL, 50.1 mmol). A 20 mL THF solution of methacryloylchloride (4.73 mL, 48.9 mmol) was added dropwise at 0 °C, and the reaction was carried out for 30 min followed by another 8 h at room temperature. A dilute ammonium chloride solution was added. After stirred for another 30 min, the mixture was evaporated, extracted 3 times with ethyl ether, and washed with 1 mol/L HCl, saturated sodium bicarbonate and brines, successively. The organic layer was dried by sodium sulfate and evaporated. The residue was purified by column chromatography (10% EtOAc/Hexanes) subsequent recrystallization to afford DKMA (10.56 g, yield = 87%) as white crystal. This compound existed as a mixture of two isomers according to ^1H NMR spectra (keto-A/enol-B = 0.06:0.94), Enol form as the major configuration. See the ESI† for NMR characterization.

Preparation of poly[4-(3-oxo-3-phenylpropanoyl)phenyl methacrylate] (PDKMAs) with different lengths. PDKMA was synthesized via RAFT using CDB as the chain transfer agent (CTA) and AIBN as the initiator. In a typical homo-polymerization, DKMA (1.0 g, 3.24 mmol), CDB (7.06 mg, 0.026 mmol), and AIBN (1.42 mg, 0.009 mmol) were dissolved in 7 mL anisole to form a crimson transparent solution, and the monomer concentration was 0.5 M. After deoxygenated by three freeze–pump–thaw cycles, the flask was sealed and immersed into a preheated oil bath at 70 °C to start the polymerization. After a predetermined time, the reaction mixture was cooled to room temperature and precipitated into cold diethyl ether. The precipitate was separated by centrifugation and dried in vacuum at 30 °C for 24 h (475 mg, 47.2%). See the ESI† for NMR characterization.

Synthesis of poly[4-(3-oxo-3-phenylpropanoyl)phenyl methacrylate]-*b*-Ploy[oligo (ethylene glycol) methyl ether methacrylate] (PDKMA-*b*-POEGMAs) diblock copolymers. PDKMA was used as macroRAFT agent, In a typical block copolymerization example, PDKMA$_{50}$ ($M_{n,nmr}$ = 15.7 kDa, 152.2 mg) OEGMA (478.4 mg, 0.956 mmol), and AIBN (0.523 mg, 0.003 mmol) as radical initiator were dissolved in anisole (10.0 mL) in a Schlenk vial and a monomer concentration of 0.8 M. After deoxygenated by three freeze–pump–thaw cycles, the tube was placed in an oil bath at 60 °C. After a predetermined time, the reaction mixture was cooled to room temperature and precipitated three times into cold diethyl ether and dried in vacuum at 30 °C to give a pink powder. (106 mg, 27.0%) See the ESI† for NMR characterization.

Gd/Eu(III)-Chelated Micellar Nanoparticle Assembly. Polymer micelles were prepared by a solvent switching method at initial concentrations of 3.3 mg/mL. PDKMA$_{152}$-*b*-POEGMA$_{310}$, PDKMA$_{69}$-*b*-POEGMA$_{43}$ and PDKMA$_{50}$-*b*-POEGMA$_{50}$ was dissolved in 2 mL THF in a spawn bottle, 1 mL of $Ln(NO_3)_3$ THF solution which containing 1.5 mg $Eu(NO_3)_3$ and 15.2 mg $Gd(NO_3)_3$ was added with continuous stirring, after which 10 mg C_2H_5ONa was added. After another 30 min vigorous stirring, the mixture was dialyzed against deionized water for 24 h by changing dialysis medium every 4h to remove THF. After dialysis, the mixture was filtered through a filter (0.45μm), and the volume was adjusted to 50 mL. Nanoparticles containing $Ln(NO_3)_3$ were labeled as PDO1, PDO2, and PDO3, respectively.

MRI Phantom Study of Gd^{3+} Containing Hybrid nanoparticles. The T_1-weighted MRI images of hybrid nanoparticles containing Gd^{3+} were performed using a 3.0-T MRI system with a specialized one-inch quadrature mouse coil (Shanghai Chenguang Medical Technologies Co., Ltd.) at 20 °C. Samples of NPDO1 were prepared in phosphate buffered saline (PBS) with a series of concentrations of 0.15, 0.20, 0.25 and 0.30 mM of total Gd^{3+}, respectively. PBS was measured as control.

The Cytotoxicity assay of Ln3+ hybrid nanoparticle was evaluated in MCF-7 cells. To assess the biocompatibility of hybrid nanoparticles, NPDO1 was used as example for cytotoxicity assay. MCF-7 cells were seeded in 96-well culture plates at a density of 0.8×10^4 cells per well in 1640 medium containing 10% FBS for 24 h. The culture medium was removed and replenished with 200μl of fresh medium containing various amounts of Ln^{3+} hybrid nanoparticles. After 48 h incubation, 20 μL CCK-8 was added in and the cells were incubated for another 1-3 hours at 37°C. Then the absorbance at a wavelength of 450 nm of each well was measured by using a microplate reader.

Confocal Laser Scanning Microscopy (CLSM) Studies. MCF-7 cells were plated on coverslips in 24-well plates at a 5×10^4 per well density. Maintained in 1640 supplemented with 10% FBS at 37 °C in a humidified atmosphere containing 5% CO_2 for 24 h, the cells were incubated with 100 μL block copolymer dispersions (1mg/mL) for 2h, 4h, 12h and 24h at 37 °C. Then removed cell culture medium and every well was also rinsed with PBS for twice and fixed with 4% paraformaldehyde for 15 min. After discarding the paraformaldehyde, the coverslips were placed under a confocal

laser scanning microscope to observe and record fluorescent images.

Results and discussion

Synthesis

A β-diketone monomer, 4-(3-oxo-3-phenylpropanoyl)phenyl methacrylate (DKMA), was prepared using an esterification reaction (Figure 1). The phenol intermediate, 1-(4-hydroxyphenyl)-3-phenylpropane-1,3-dione, was synthesized as reported.[29] It was directly converted into DKMA monomer by treatment with methacryloylchloride in a facile substitution reaction. The crude product was purified by column chromatography and subsequent recrystallization to become spectroscopically pure monomers as white crystalline solids. The overall yield was ca. 74% from 1-(4-hydroxyphenyl)ethanone. DKMA was fully characterized by ^{1}H NMR (Figure 1A and S1 ESI†). The characteristic signals of methacrylate protons are observed at 6.39, 5.80 and 2.08 ppm. The singlet signals at 16.87 and 6.84 ppm belong to enol H^{e,d} and methyne H^c protons presenting an equilibrium with diketone. The enol form is the major isomer with the fraction of 94%, i.e. the ratio of [enol] /[keto] is 0.94: 0.06 in monomer according to the integration. ^{13}C NMR spectrum of DKMA is shown in Figure S2 ESI†.
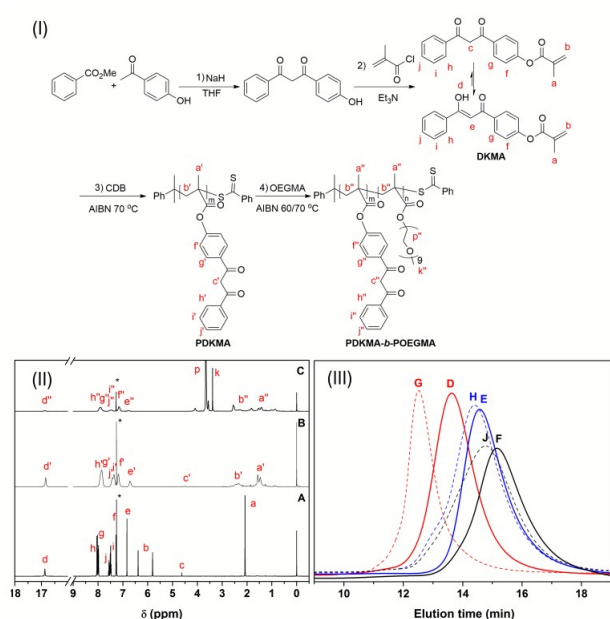
Figure 1. (I) Synthesis of diketone-containing monomer and block copolymers from 1-(4-hydroxyphenyl)ethanone. (II) ^{1}H NMR spectra of DKMA (A), PD2 (B) and PDO3 (C) with the assignments in (I), *: residue CHCl$_3$ in solvent CDCl$_3$. (III) SEC traces of homo-polymers of PD1 (D), PD2 (E) and PD3 (F) in solid lines, and block co-polymers of PDO1 (G), PDO2 (H) and PDO3 (J) in dash lines.

RAFT polymerization with chain transfer agent (CTA) of cumyl dithiobenzoate (CDB) was chosen to polymerize DKMA in a controlled way while ATRP is not applicable due to strong coordination of copper catalyst by diketone side groups of the monomer. Well-defined homo-polymers poly[4-(3-oxo-3-phenylpropanoyl)phenyl] (PDKMA) and diblock copolymers poly[4-(3-oxo-3-phenylpropanoyl)phenyl methacrylate]-b-poly[oligo(ethylene glycol) methyl ether methacrylate] (PDKMA-b-POEGMA) named as PD and PDO in Table 1, respectively, were synthesized with different chain lengths. The MWs measured by SEC and ^{1}H NMR spectroscopy (Table 1, Figures 1, S3 and S4 ESI†) agreed well with the corresponding theoretical values indicating well controlled RAFT polymerizations. As shown in Figures 1B and S3, the ratio of enol/kitone in PDKMA is calculated as 94.6:5.4 by the integrals of proton signals at 16.87 and 4.50 ppm indicating the equilibrium is not changed after polymerization. The protons of aromatic rings (H$^{f', g', h', i', j'}$ at 7.86-7.18 ppm) and backbone (H$^{b'}$ and H$^{a'}$ between 2.44 and 1.43 ppm) of PDKMA are observed.

PDKMAs with MWs ranging from 12.8 to 33.8 kDa and moderate polydispersity indices (Đ < 1.30) were obtained by varying the feed ratio of [DKMA]/[CDB] (Table 1). We kept monomer conversions low (40-65%) for better polymerization control. In all SEC measurements, the polystyrene-calibrated MWs were significantly lower than theoretical values consistent with the structural difference between PDKMA and the polystyrene standards.[30] Indeed, the absolute M_n of PDKMA$_{152}$ was determined by multi-angle laser light scattering (MALLS) as 47.1 kDa quite close to the expected value (Figure S5 ESI†).

Homo-polymer PDKMAs containing dithioester chain end were used as macro-CTA in the RAFT polymerizations of OEGMA to produce PDKMA-b-POEGMAs. Figure 1C illustrates a typical ^{1}H NMR spectrum of the block copolymers and the details are shown in Figure S4 ESI†. Both the typical proton signals of DKMA and OEGMA units are found. The signal at 16.90 ppm indicates enol proton of PDKMA and the signals among 7.89-6.74 ppm are attributed to the aromatic protons. OEGMA segment shows the characteristic signals at 4.08 ppm, 3.65 ppm and 3.38 ppm. PDKMA-b-POEGMAs have been successfully synthesized. The block lengths and compositions are calculated from the intensities of the ethyl groups of POEGMA (H$^{p'}$) and the aryl group of PDKMA (H$^{f'', g'', h'', i'', j''}$). Figure 1 illustrates the SEC profiles of the PDKMA-b-POEGMAs with MWs ranging from 18.2 to 79.8 kDa and the corresponding PDKMA precursors. Obvious MW increase of PDKMA-b-POEGMAs compared with PDKMA precursors, as well as the symmetrical and mono-modal peaks, indicates that all PDKMA chain ends propagated with OEGMA monomers.

According to TGA under inert atmosphere (Figure S6 ESI†), decomposition temperatures (T_ds, the temperature at 5% weight loss) of PD1, PD2 and PD3 are 262.8, 277.0 and 214.6 °C, respectively, showing good thermal stabilities of the

polymers. In a typical DSC profiles of PD1 (Figure S7 ESI†), PDKMAs have two glass transitions at T_gs of about 117.0 and 150.3 °C. The former responds to side chain slip associated with the destruction of π-π stacking between aromatic groups and hydrogen bonding between diketone groups. The latter is a movement of polymer backbone. Corresponding block copolymers also exhibit two T_gs at 122.6 and 149.6 °C indicating that the block copolymers are phases separating in the bulk. Melting temperatures (T_m) at -5.5 °C (sample PDO1 Figure S7 ESI†) are slightly near the homo-polymer of POEGMA.

Table 1. RAFT homo- and block co-polymerization of DKMA.

| Sample	Polymers	[M]/[CTA]/[I]$^{a)}$	Time (h)	Temp. (°C)	Conv.$^{b)}$ (%)	$M_{n, calc}$ (kDa)$^{c)}$	$M_{n,SEC}$ (kDa)$^{d)}$	$Đ^{d)}$
PD1	PDKMA$_{152}$$^{e)}$	900/3/1	10.5	70	52	47.1	33.8	1.28
PD2	PDKMA$_{69}$$^{b)}$	300/3/1	10.0	70	69.3	21.5	16.3	1.30
PD3	PDKMA$_{50}$$^{b)}$	300/3/1	7.5	70	49.5	15.7	12.8	1.30
PDO1	PDKMA$_{152}$-b-POEGMA$_{310}$$^{f)}$	900/3/1	3.7	70	77.4	202.1	79.8	1.33
PDO2	PDKMA$_{69}$-b-POEGMA$_{43}$$^{f)}$	375/3/1	11.2	60	29	43.0	20.8	1.33
PDO3	PDKMA$_{50}$-b-POEGMA$_{50}$$^{f)}$	300/3/1	6.0	60	30	40.7	18.2	1.36

a) Molar ratio of monomer (M), CTA (CDB or PDKMAs) and AIBN (I) in feed. b) Trioxymethylene was taken as an initial sample to monitor the conversion by ^{1}H-NMR spectroscopy, and DP was measured by comparing the experimental conversion with desired conversion. c) $M_{n, calc} = M_{monomer} \times ([M]/[CTA]) \times Conversion + M_{CTA}$. d) Determined from SEC in THF calibrated by PS standards. e) M_n was determined by MALLS. f) PDKMA-b-POEGMAs composition determined by ^{1}H NMR according to [DKMA]/[OEGMEMA] = I(Ar$\underline{H}$)/I(OC$\underline{H_2}$C$\underline{H_2}$O).

Micellization

The amphiphilic block copolymers self-assemble into micelles in aqueous solution with PDKMA core and POEGMA shell with a typical solvent-switching method. The critical micelle concentration (CMC) values of PDO1, PDO2 and PDO3 are $2.63×10^{-2}$, $1.59×10^{-4}$ and $1.67×10^{-4}$ mg/mL, respectively, as monitored by the fluorescent method using pyrene as a probe (Figure S8 ESI†).[31-33] The high CMC value of PDO1 contributes to the high ratio of hydrophobic PDKMA segment and water-soluble POEGMA fraction. Higher ratios of hydrophobic and hydrophilic fractions, i.e. relatively shorter POEGMA segments, decrease the CMC values of PDO2 and PDO3 into the magnitude of 10^{-4} mg/L facilitating stable formation of aqueous micelles.

The chelation of lanthanide (Ln) cations was done by nanoprecipitation method. Into a THF solution of PDKMA-b-POEGMA, Eu(NO$_3$)$_3$ and Gd(NO$_3$)$_3$ mixture was added dropwise under continuous stirring and followed by C$_2$H$_5$ONa/THF solution. The mixtures were dialyzed against deionized water to form Ln-hybrid nanoparticles that were denoted as NPDO1, NPDO2 and NPDO3 obtained from PDO1, PDO2 and PDO3, respectively. The hydrodynamic volumes and morphologies of the nanoparticles were analyzed by dynamic light scattering (DLS) and transmission electron microscopy (TEM) in Figure 2. NPDO1 and NPDO3 micelles obtained from PDO1 and PDO3 have the diameters of 222 nm (PDI = 0.084) and 87 nm (PDI = 0.145), respectively, with uniform sizes and homogeneous distributions. The zeta potential of NPDO1 and NPDO3 is -0.5 mv and -19 mv, respectively. In contrast, a few large and polydisperse aggregates in NPDO2 indicate unstable assembly after chelation of Ln^{3+} cations of PDO2 (Figure S9 ESI†). The hydrophilic POEGMA segment in PDO2 is the shortest among the three that is not long enough to stabilize micelles stably. In contrary, micelles (NPDO1 and NPDO3) show clear contrast between the dark staining background and white spots in TEM confirming remarkably uniformly sized spheres with nearly average diameters of 30 and 20 nm. It is reasonable that the diameters of the micelles obtained from TEM are smaller than the corresponding DLS data since POEGMA shell cannot be observed in TEM. In addition, TEM pictures nanoparticles in dehydrated solid states while DLS measures hydrodynamic diameters of micelles swollen in an aqueous environment.[34]
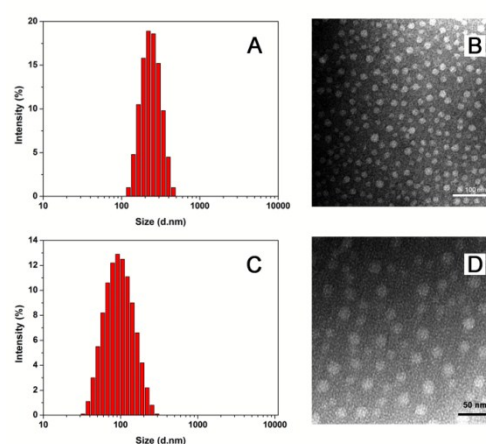
Figure 2. Size distributions histograms (A and C) and TEM images (B and D) of NPDO1 (A and B) and NPDO3 (C and D) nanoparticles in aqueous media at 25 °C. The scale bars in B and D are 100 and 50 nm, respectively.

The chelation of lanthanide assemblies is confirmed by comparing block copolymer PDO1 and the corresponding NPDO1 nanoparticles using FT-IR analysis (Figure S10 ESI†). Strong absorbent bands at 1601 and 1490 cm^{-1} in PDO1 attributes to the stretching vibrations of C=O and C=C (enol isomer) in β-diketone groups, respectively.[35] Their red shift to 1596 and 1473_cm^{-1} in NPDO1 suggests the coordination of carbonyl group to lanthanide cations. The C–O vibration from C=C–O–H(Ln) exhibits medium intensity absorption at 1301 cm^{-1} in PDO1 which dramatically red shifts to 1259 cm^{-1} after the deprotonation of enol hydroxyl group and reaction with Ln^{3+} ions. A medium-to-weak band at 437 cm^{-1} is observed as an additional evidence of the Ln–O formation.[36]

The inductively coupled plasma optical emission spectrometry (ICP-OES) quantitatively reveals the Ln^{3+} concentration in the NPs solution (Table S1 ESI†). The contents of Gd^{3+} are 52.88 and 14.72 μg/L in NPDO1 and NPDO3, respectively. As fluorescent imaging is more sensitive than MRI and Gd^{3+} also sensitizes Eu^{3+} efficiently, we control the concentration of Eu^{3+} lower than Gd^{3+} in half to one magnitude on purpose.

The chelation stability of Ln^{3+} ions takes the risk of leaking from micelles whose shell is non-crosslinked and hydrophilic POEGMA shell. To measure the leakage of Ln^{3+} cations, NPDO1 and NPDO3 nanoparticles were dialyzed against deionized water for a week and the dialysis fluids were submitted to ICP-OES. The free Gd^{3+} and Eu^{3+} concentrations were far below the detection limit of the ICP-AES (i.e., 1 μg/L). Our hybrid NPs provide a very stable chelation of Ln^{3+}, indicating application potential as safe nanomaterials.

MRI Phantom Study

Gadolinium species are well-known candidates as longitudinal (T_1-type) relaxation MRI contrast agent which can vastly improve the diagnostic sensitivity toward malignant tissues over normal ones.[37-39] Meanwhile, the gadolinium complex often suffers from limited sensitivity.[40, 41] In an effort to improve the contrast performances, the macromolecular Gd^{3+} complexes which are covalently conjugated onto polymers or polymer assemblies have been reported by several previous literature.[42] We herein synthesize a novel kind of Gd^{3+} hybrid polymer micelle with increased T_1 relaxivity for MRI. From the plots of the $1/T_1$ against the Gd^{3+}-concentration, as shown in Figure 3, the longitudinal relaxivity (r_1) of NPDO1 was determined as 11.2 mM^{-1}s^{-1} using a 3.0 T magnetic field at 20 °C. It is noteworthy that the r_1 value of this Gd^{3+}-chelated polymer micelle reaches nearly 3-fold enhancement compared with commercial small molecular contrast agent Gd-DOTA (3.8 mM^{-1}s^{-1}) or Gd-DTPA (4.0 mM^{-1}s^{-1}).[43-45] With higher T_1 contrast efficiency, a lower dose of NPDO1 can achieve a comparable T_1 contrast enhancement. Same polymer-based enhancements have been reported with careful designs. Compared with other polymeric Gd^{3+}-based nanoparticles reported, the r_1 value of NPDO1 is comparable and moderate.[46-50] Typical T_1-weighted spin-echo MR images recorded for Gd^{3+}-chelated polymer micelle (NPDO1) at various concentrations in phosphate buffered saline (PBS) are shown in the inset of Figure 3. By gradually increasing the concentration of NPDO1, a lightly positive enhancement spot

brightness can be observed. PBS was measured as a control showing a darkest spot.
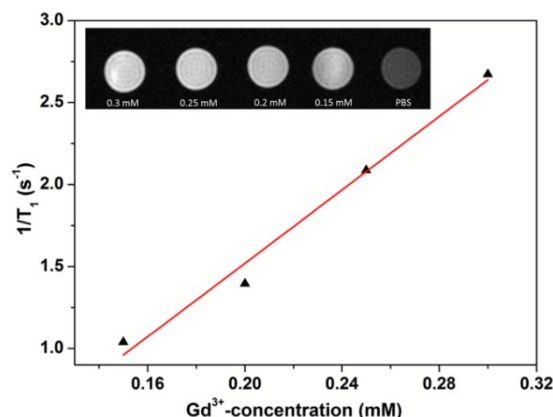
Figure 3. Plots of longitudinal ($1/T_1$) for aqueous solutions of Gd^{3+}-chelated polymer micelle (NPDO1) at various concentrations, inset: T_1-weighted spin-echo MR images recorded in versus Gd^{3+}-concentrations of NPDO1 and PBS was measured as references.

UV and fluorescence

The UV-Vis absorption spectra of PDO1 micelles with and without lanthanide cations in aqueous solution were recorded in Figure 4A (similar results of PDO3 and NPDO3 are shown in Figure S11 ESI†). A broad absorption band between 295 and 420 nm with maximum at 340 nm is expected as the π–π * singlet-singlet transition to the excited state. The π–π* transition bands centered on the diketone moiety experience a red shift of ca. 10-20 nm compared with that of the free diketone chromophore, implying an electronic interaction between the light-absorbing diketone and the light-emitting center (Ln^{3+}).[51]
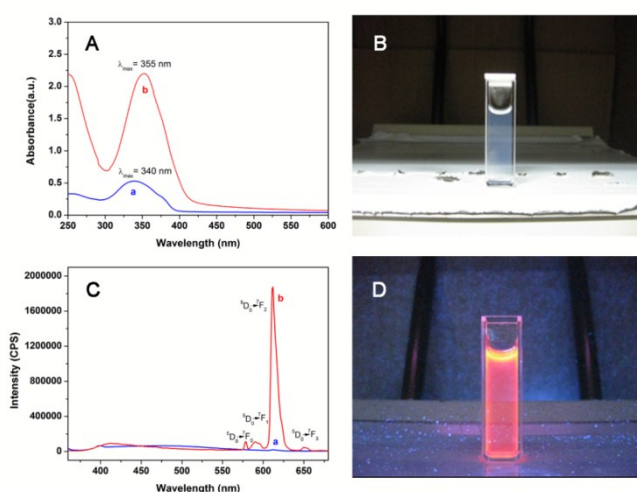

Figure 4. (A) UV-Vis of 0.04 mg/mL PDO1 (a) and 0.073 mg/mL PDO1 with Ln^{3+} (b) in aqueous media; (B) Photographs of solution NPDO1 under sunlight; (C) PL spectra of PDO1 (4×10^{-4} mg/mL, curve a) and NPDO1 (6.6×10^{-4} mg/mL, curve b) in aqueous solution under

excitation at 350 nm at 25 °C; (D) Photographs of solution NPDO1 under UV lamp at 365 nm.

The emission spectra of the hybrid nanoparticles give out typical narrow-band Eu^{3+} luminescence in the region 570–680 nm after excitation at 350 nm (Figures 4C and S12 ESI†). The hydrophobic character of PDKMA core prevents quenching by water accessing to the coordinated lanthanide ions and therefore keeps efficient fluorescence output. The luminescence and the corresponding emission spectra demonstrating that energy transfer from the aromatic β-diketonate ligand to Eu^{3+} center is responsible for the sensitized europium emission of narrow bands at 579 (J = 0), 590 (J = 1), 614 (J = 2) and 650 (J = 3) nm correspond to the $^5D_0 \rightarrow ^7F_J$ f-f transitions in Eu^{3+}.[52] The aromatic ligand is first excited to its S_1 state, after intersystem crossing, energy transfers to the triplet state, then the energy transfers to $^5D_1$ state of Eu^{3+} via the ligand triplet state. Since the $^5D_1$ state finally emits fluorescence via $^5D_0$, the fluorescent spectra of Eu^{3+} is always the same and independent from the ligands. The electronic dipole transitions $^5D_0 \rightarrow ^7F_2$ at 614 nm is the strongest, so-called "hypersensitive" transition being the most intense.[52] The lanthanide-polymer complexes possess a large Stokes shift ($\lambda_{em} - \lambda_{exc}$) of over 200 nm while that of organic dyes is typically less than 50 nm. The effect of Gd^{3+} ions as a heavy atom on the luminescence properties of Eu^{3+} which can efficiently enhance the luminescence of Eu^{3+} ions, so the intensity of characteristic Eu^{3+} emission is largely increased.[2, 15, 16]

Cytotoxicity assay

The cytotoxicity of lanthanide hybrid nanoparticles was evaluated in MCF-7 cells (human breast adenocarcinoma cell line) by measuring the inhibition of cell growth using CCK-8 assay. The relative cell viability was determined by comparing the absorbance at 450 nm with that of control wells containing only cell culture medium. Data are presented as average (SD (n = 5)). Figure 5 illustrates MCF-7 cells cultivated for 48 h with various concentrations of Ln^{3+} hybrid nanoparticles from 0 to 800 μg/mL. The high cell viability over 90% indicates very low toxicity with MCF-7 cells.
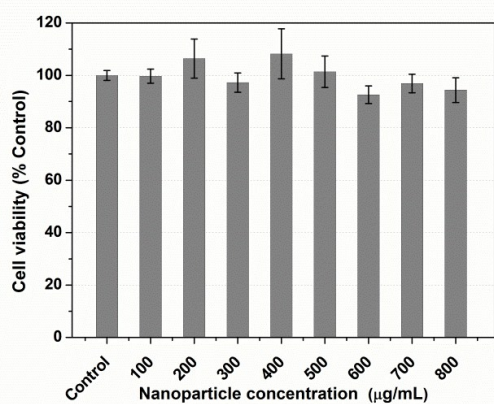
Figure 5. Relative cell viability of NPDO1 for MCF-7 cells after 48 h incubation at a concentration between 0 to 800 μg/mL.

Cellular uptake studied by confocal microscopy

The NPDO1 nanoparticles can be absorbed by MCF-7 cells observed by confocal laser scanning microscope (CLSM) with the excitation wavelength of 405 nm and emission wavelength of 620 nm probed by Eu^{3+} fluorescent imaging. As shown in Figure 3, the intensity of cellular uptake was time-dependently increasing from 2 h to 24 h of incubation. Low cytotoxicity and excellent cellular uptake ability make the lanthanide hybrid nanoparticles a favorable vector applied in biomedical imaging, especially suitable for assessing thin biopsies in confocal imaging.
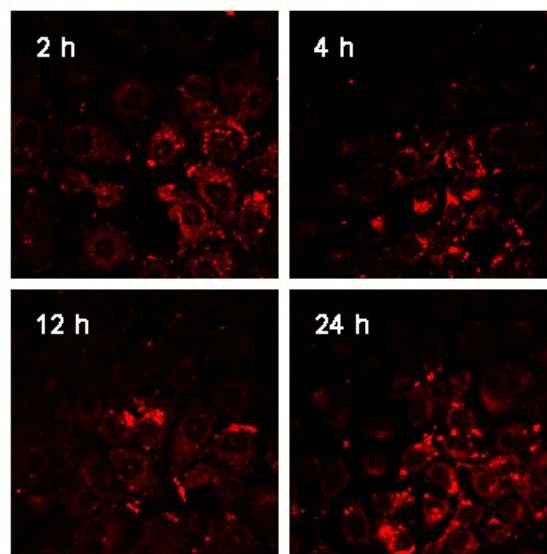
Figure 6. CLSM images of MCF-7 cells incubated with NPDO1 for 2~24 h at 37 °C under excitation at 405 nm.

Conclusions

In this study, we synthesized a series of innovative β-diketone micelles with a homogeneous size distribution based on amphiphilic block copolymer (PDKMA-*b*-POEGMA) chelating Gd^{3+} and Eu^{3+} cations. The sizes of lanthanides hybrid micelles are in the range of 87 and 222 nm capable for accumulation in tumors via the enhanced permeability and retention effect. They exhibit combined properties of both MRI and red fluorescence imaging demonstrated by CLSM and in vitro relaxivity studies. The large Stokes shift in fluorescence can avoid the overlapping with biological background. Eu^{3+} luminescence outputs efficiently and suffers less from non-radiative deactivation. Meanwhile, the relaxivity values are 3-folded higher than commercial DOPA- and DTPA-Gd^{3+} agents, which can be attributed to outer sphere water exchange with Gd^{3+} and conjugated to macromolecules. The hybrid micelles are kinetically stable with negligible leaching of Ln^{3+} ions into solution. Biocompatibility studies evidenced the non-toxicity and the safe use of such lanthanide chelated nanoparticles in cell studies. In short, the Gd/Eu micelles constitute a highly versatile platform and highly contrast agent for the

simultaneous optimization of both MRI and fluorescence properties in one single probe suggesting endless potential applications for theranostics, early diagnosis of tumor, and intraoperative fluorescence-guided surgery.
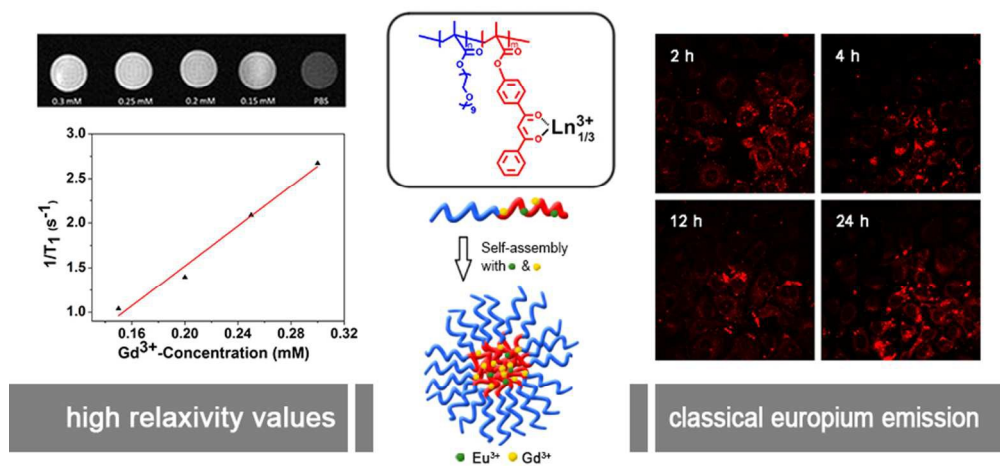
Acknowledgements

Notes and references

1. Y. Wang, L. Ji, B. Zhang, P. Yin, Y. Qiu, D. Song, J. Zhou and Q. Li, *Nanotechnology*, 2013, **24**, 175101.

2. D. J. Lewis, F. Moretta and Z. Pikramenou, *Supramol. Chem.*, 2012, **24**, 135-142.

3. L. Pellegatti, J. Zhang, B. Drahos, S. Villette, F. Suzenet, G. Guillaumet, S. Petoud and É. Tóth, *Chem. Commun.*, 2008, **48**, 6591-6593.

4. D. Shi, H. S. Cho, Y. Chen, H. Xu, H. Gu, J. Lian, W. Wang, G. Liu, C. Huth, L. Wang, R. C. Ewing, S. Budko, G. M. Pauletti and Z. Dong, *Adv. Mater.*, 2009, **21**, 2170-2173.

5. J. Gao, H. Gu and B. Xu, *Acc. Chem. Res.*, 2009, **42**, 1097-1107.

6. Y. Ge, Y. Zhang, S. He, F. Nie, G. Teng and N. Gu, *Nanoscale Research Letters*, 2009, **4**, 287-295.

7. D. Shi, *Adv. Funct. Mater.*, 2009, **19**, 3356-3373.

8. W. Cai and X. Chen, *Small*, 2007, **3**, 1840-1854.

9. J.-H. Park, G. von Maltzahn, E. Ruoslahti, S. N. Bhatia and M. J. Sailor, *Angew. Chem., Int. Ed.*, 2008, **47**, 7284-7288.

10. L. H. a. T. André Merbach and L. H. a. M. éva Tóth, in *The Chemistry of Contrast Agents in Medical Magnetic Resonance Imaging, Second Edition*, 2013, pp. 25-82.

11. A. Picot, A. D'Aleo, P. L. Baldeck, A. Grichine, A. Duperray, C. Andraud and O. Maury, *J. Am. Chem. Soc.*, 2008, **130**, 1532-1533.

12. P. G. Sammes and G. Yahioglu, *Natural Product Reports*, 1996, **13**, 1-28.

13. H. Liang, Q. J. Zhang, Z. Q. Zheng, H. Ming, Z. C. Li, J. Xu, B. Chen and H. Zhao, *Opt. Lett.*, 2004, **29**, 477-479.

14. C. Pettinari, F. Marchetti, R. Pettinari, A. Drozdov, S. Troyanov, A. I. Voloshin and N. M. Shavaleev, *Journal of the Chemical Society-Dalton Transactions*, 2002, **7**, 1409-1415.

15. Y. Wu, Y. Zhou, O. Ouari, M. Woods, P. Zhao, T. C. Soesbe, G. E. Kiefer and A. D. Sherry, *J. Am. Chem. Soc.*, 2008, **130**, 13854-13855.

16. C. Lin, Y. Song, F. Gao, X. Zhou, Y. Sheng, Z. Shi and H. Zou, *J. Lumin.*, 2015, **158**, 456-463.

17. K. W.-Y. Chan and W.-T. Wong, *Coord. Chem. Rev.*, 2007, **251**, 2428-2451.

18. P. Caravan, J. J. Ellison, T. J. McMurry and R. B. Lauffer, *Chem. Rev.*, 1999, **99**, 2293-2352.

19. L. Thunus and R. Lejeune, *Coord. Chem. Rev.*, 1999, **184**, 125-155.

20. C. S. Bonnet, F. Buron, F. Caille, C. M. Shade, B. Drahoš, L. Pellegatti, J. Zhang, S. Villette, L. Helm, C. Pichon, F. Suzenet, S. Petoud and É. Tóth, *Chemistry-a European Journal*, 2012, **18**, 1419-1431.

21. S. Laurent, L. V. Elst, M. Wautier, C. Galaup, R. N. Muller and C. Picard, *Bioorganic & Medicinal Chemistry Letters*, 2007, **17**, 6230-6233.

22. A. J. L. Villaraza, A. Bumb and M. W. Brechbiel, *Chem. Rev.*, 2010, **110**, 2921-2959.

23. P. Lebdušková, J. Kotek, P. Hermann, L. V. Elst, R. N. Muller, I. Lukeš and J. A. Peters, *Bioconjugate Chem.*, 2004, **15**, 881-889.

24. C.-H. Huang, K. Nwe, A. Al Zaki, M. W. Brechbiel and A. Tsourkas, *Acs Nano*, 2012, **6**, 9416-9424.

25. Y. Li, M. Beija, S. Laurent, L. vander Elst, R. N. Muller, H. T. T. Duong, A. B. Lowe, T. P. Davis and C. Boyer, *Macromolecules*, 2012, **45**, 4196-4204.

26. K. Luo, G. Liu, W. She, Q. Wang, G. Wang, B. He, H. Ai, Q. Gong, B. Song and Z. Gu, *Biomaterials*, 2011, **32**, 7951-7960.

27. E. Debroye, S. V. Eliseeva, S. Laurent, L. V. Elst, R. N. Muller and T. N. Parac-Vogt, *Dalton Transactions*, 2014, **43**, 3589-3600.

28. G. Moad, J. Chiefari, Y. K. Chong, J. Krstina, R. T. A. Mayadunne, A. Postma, E. Rizzardo and S. H. Thang, *Polym. Int.*, 2000, **49**, 993-1001.

29. H. Jin, W. Zhang, D. Wang, Z. Chu, Z. Shen, D. Zou, X. Fan and Q. Zhou, *Macromolecules*, 2011, **44**, 9556-9564.

30. F. Cheng and F. Jäkle, *Chem. Commun.*, 2010, **46**, 3717-3719.

31. Z. Wang, M. Gao, J. Sun, D. Liang and X. Jia, *Macromolecules*, 2013, **46**, 1723-1731.

32. M. Wilhelm, C. L. Zhao, Y. C. Wang, R. L. Xu, M. A. Winnik, J. L. Mura, G. Riess and M. D. Croucher, *Macromolecules*, 1991, **24**, 1033-1040.

33. W. Wang, L. Chang, X. Li, Y. Wu, J. Xing, L. Deng and A. Dong, *Soft Matter*, 2012, **8**, 1575-1583.

34. Y. Li, H. Guo, Y. Zhang, J. Zheng, J. Gan, X. Guan and M. Lu, *RSC Advances*, 2014, **4**, 17768-17779.

35. Y.-M. Luo, J. Li, L.-X. Xiao, R.-R. Tang and X.-C. Tang, *Spectrochimica Acta Part a-Molecular and Biomolecular Spectroscopy*, 2009, **72**, 703-708.

36. J. Pei, X. L. Liu, W. L. Yu, Y. H. Lai, Y. H. Niu and Y. Cao, *Macromolecules*, 2002, **35**, 7274-7280.

37. Q. Zheng, H. Q. Dai, M. E. Merritt, C. Malloy, C. Y. Pan and W. H. Li, *J. Am. Chem. Soc.*, 2005, **127**, 16178-16188.

38. G. Liang, J. Ronald, Y. Chen, D. Ye, P. Pandit, M. L. Ma, B. Rutt and J. Rao, *Angew. Chem., Int. Ed.*, 2011, **50**, 6283-6286.

39. D. T. Schühle, P. van Rijn, S. Laurent, L. Vander Elst, R. N. Muller, M. C. A. Stuart, J. Schatze and J. A. Peters, *Chem. Commun.*, 2010, **46**, 4399-4401.

40. K. Kono, S. Nakashima, D. Kokuryo, I. Aoki, H. Shimomoto, S. Aoshima, K. Maruyama, E. Yuba, C. Kojima, A. Harada and Y. Ishizaka, *Biomaterials*, 2011, **32**, 1387-1395.

41. K. Shiraishi, K. Kawano, T. Minowa, Y. Maitani and M. Yokoyama, *J. Controlled Release*, 2009, **136**, 14-20.

42. E. Battistini, E. Gianolio, R. Gref, P. Couvreur, S. Fuzerova, M. Othman, S. Aime, B. Badet and P. Durand, *Chemistry-a European Journal*, 2008, **14**, 4551-4561.

43. D. H. Powell, O. M. NiDhubhghaill, D. Pubanz, L. Helm, Y. S. Lebedev, W. Schlaepfer and A. E. Merbach, *J. Am. Chem. Soc.*, 1996, **118**, 9333-9346.

44. Z. Zhou, L. Wang, X. Chi, J. Bao, L. Yang, W. Zhao, Z. Chen, X. Wang, X. Chen and J. Gao, *Acs Nano*, 2013, **7**, 3287-3296.

45. Q. Liu, S. Chen, J. Chen and J. Du, *Macromolecules*, 2015, **48**, 739-749.

46. Z. Zhou and Z.-R. Lu, *Wiley Interdisciplinary Reviews-Nanomedicine and Nanobiotechnology*, 2013, **5**, 1-18.

47. Z. Zhou and Z.-R. Lu, *Nanomedicine*, 2014, **9**, 2387-2401.

48. M. Tan, Z. Ye, D. Lindner, S. M. Brady-Kalnay and Z.-R. Lu, *Pharm. Res.*, 2014, **31**, 1469-1476.

49. C. F. G. C. Geraldes and S. Laurent, *Contrast Media & Molecular Imaging*, 2009, **4**, 1-23.

50. G. Zhang, R. Zhang, X. Wen, L. Li and C. Li, *Biomacromolecules*, 2008, **9**, 36-42.

51. L. Tei, G. Mazooz, Y. Shellef, R. Avni, K. Vandoorne, A. Barge, V. Kalchenko, M. W. Dewhirst, L. Chaabane, L. Miragoli, D. Longo, M. Neeman and S. Aime, *Contrast Media & Molecular Imaging*, 2010, **5**, 213-222.

52. Y.-Y. Li, B. Yan and Q.-P. Li, *Dalton Transactions*, 2013, **42**, 1678-1686.

80x39mm (300 x 300 DPI)